Poly(styrene-*block*-butadiene-*block*-styrene-*block*-butadiene) and Poly(styrene-*block*-butadiene-*block*-methyl methacrylate) Copolymers as Compatibilizers in PPO–SAN Blends. I. Morphology and Fracture Behavior

R. LACH,[1] W. GRELLMANN,[1] R. WEIDISCH,[2] V. ALTSTÄDT,[3] T. KIRSCHNICK,[3] H. OTT,[3] R. STADLER,[4] C. MEHLER[5]

[1] Martin-Luther-Universität Halle-Wittenberg, Institut für Werkstoffwissenschaft, D-06099 Halle, Germany

[2] Max-Planck-Institut für Polymerforschung, D-55021 Mainz, Germany

[3] Technische Universität Hamburg-Harburg, Arbeitsbereich Kunststoffe und Verbundwerkstoffe, D-21071 Hamburg, Germany

[4] Universität Bayreuth, Lehrstuhl für Makromolekulare Chemie II, D-95440 Bayreuth, Germany

[5] BASF AG, D-67056 Ludwigshafen, Germany

Received 25 May 1999; accepted 29 October 1999

ABSTRACT: The toughness behavior of PPO–SAN blends with the modifier poly(styrene-*block*-butadiene) (SBSB) and with poly(styrene-*block*-butadiene-*block*-methyl methacrylate) copolymers (SBM) under impact loading conditions has been investigated. The observed morphology of blends compatibilized with SBM, in which the rubber phase discontinuously accumulated at the PPO–SAN interface, correlated with about 20 times higher energy dissipation up to maximum force and about seven times higher deformation capacity compared to pure PPO–SAN blends. In contrast, the fracture behavior of the SBSB-modified blends was not as strongly dependent on the rubber content. It is especially noteworthy that although the SBM modification resulted in a strong increase in toughness of the PPO–SAN blends, no decrease in stiffness could be found with up to 15% rubber additions. The values of Young's moduli remained at the same high level of the nonmodified material. © 2000 John Wiley & Sons, Inc. J Appl Polym Sci 78: 2037–2045, 2000

Key words: fracture mechanics; Charpy impact test; PPO–SAN blends; block copolymers; compatibilization

INTRODUCTION

Improving mechanical behavior (i.e., stiffness, strength, and toughness) has been a major goal in polymer research. However, it is often observed that the optimization of one mechanical property occurs at the expense of others. For example, although the toughness of brittle polymers is generally increased by modification with rubber, such modification also results in reduced stiffness and strength (Fig. 1).[1] The toughened polymeric systems produced in this way are not useful for structural applications. Therefore, it is necessary

Correspondence to: R. Lach (wolfgang.grellmann@iw.uni-halle.de).

Contract grant sponsor: Bundesministerium für Bildung und Forschung; contract grant number: 03-M-4086-1.

Journal of Applied Polymer Science, Vol. 78, 2037–2045 (2000)

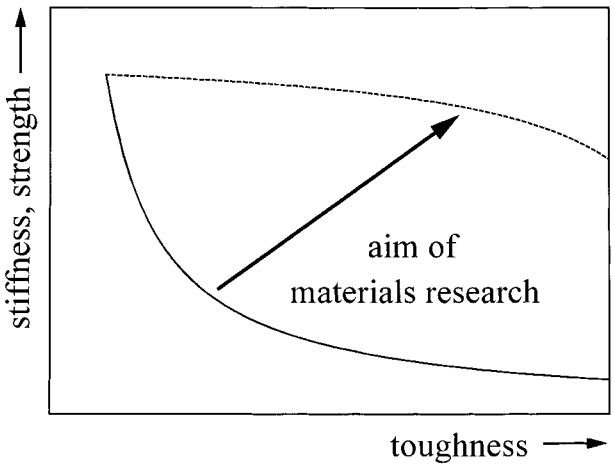

Figure 1 Schematic representation of the observed and desired mechanical behavior–toughness relationship. Full line: mechanical behavior of conventional toughened polymeric materials. Broken line: mechanical behavior of polymeric materials for constructive applications.

to develop novel strategies for enhancing toughness in order to allow for new applications for polymeric materials. One possible approach for toughening a polymer while retaining a high stiffness is to incorporate a suitable stiff polymeric modifier into a sufficiently stiff matrix material, using an appropriate block copolymer as a phase compatibilizer.

The use of poly(styrene-*block*-methyl methacrylate) copolymers (SM) as coupling agents in PPO–SAN blends has been reported in earlier works.[2,3] However, these studies were largely focused on evaluating the effectiveness of SM for the dispersion of SAN into the PPO matrix and the formation of the blend morphology (particle diameter and form and interface thickness).[2,3]

In this paper the influence of the phase-coupling behavior of block copolymers containing a rubber blocklike poly(styrene-*block*-butadiene-*block*-styrene-*block*-butadiene) (SBSB) and poly (styrene-block-butadiene-block-methyl methacrylate) (SBM) on the mechanical as well as fracture properties of PPO–SAN blends is discussed. The influence of the composition, molecular weight, and content of block copolymers on such mechanical behavior has been examined. Important aspects of this work are the correlations between the macroscopic fracture and deformation behavior with structural parameters and micro-mechanical deformation processes.

Bulk SBM triblock copolymers exhibit a variety of ordered morphologies depending on the length of the constituent blocks. For example, a lamellar structure for the PS and PMMA phase has been reported.[4] In this morphology, the polybutadiene (PB) resides at the interface between the lamellae as spheres (i.e., a ball-at-the-wall structure). Stadler et al.[5] reported on the formation of PS cylinders in a PMMA matrix. Different types of PB structures were described in this work, including a continuous PB phase present as shells around PS cylinders and PB phases in the forms of cylinders, rings, helices, or also spheres at PS–PMMA interfaces. The ball-at-the-wall structure described by Beckmann et al.[4] is a particularly suitable description of the morphology of PPO–SAN blends compatibilized with SBM.

Because of the immiscibility of PB with all other blend components and the miscibility of PPO with PS and SAN with PMMA, respectively, SBM is concentrated at the PPO–SAN interface. Hence, the phase separation of micron-sized PB spheres with a morphology comparable to the ball-at-the-wall structure has been observed. Discrete, spherical PB particles are produced at the interfaces of these two kinds of lamellar-type structures (PPO–PS "lamellae" near the PPO particles and SAN/PMMA "lamellae" near the SAN matrix). In the literature,[6] such a phase distribution has been described as the "raspberry" morphology.

Auschra et al.[3] investigated the compatibilization of PPO and SAN using a symmetric poly(styrene-*block*-methyl methacrylate) copolymer (SM; molecular weight M_n = 100 kg/mol). The observed diameters of particles comprised of PPO–PS mixtures ranged from 78 to 85 nm. The value of the linear chain-stretching factor, calculated by comparing this observed diameter with the long period (66 nm) of a pure SM (lamellar morphology; M_n = 100 kg/mol),[7] was about 2.5.[3] In light of this observation, the present authors hypothesized that similar conditions may be valid for PPO–SAN blends compatibilized with SBM.

EXPERIMENTAL

Specimen Preparation

The materials used in this study are presented in Table I. SAN with 19% acrylonitrile content, PPO–HIPS with 28,5% HIPS, and a symmetrical SBM or a SBSB were used.

The SBM block copolymer was prepared by sequential anionic polymerization.[8] The polymerization of polystyrene was initiated in ethylben-

Table I Materials

Materials	M_W (g/mol)	Form
SAN	244,000	granules
PPO	40,000	powder
SBM	130,000	powder
SBSB	68,000	granules

zene at 60°C with s-BuLi. After the complete consumption of the styrene, 1,3-butadiene was added. The reactor was cooled down to 0°C, and diphenylethylene was added to lower the reactivity of the living chain end for the following polymerization of MMA at −20°C. As a result of using ethylbenzene as the solvent during anionic polymerization of the SBM–copolymer, the midblock consisted predominantly (82.9%) of 1,4-PB.

The SBSB block copolymer was composed of 43% styrene and 40% 1,2-PB. With the exception of SBSB (a commercial product of Asahi Chemical Industry Co., Mizushima, Japan), all materials were provided by BASF AG (Ludwigshafen, Germany).

After mechanical mixing, the blend components were compounded using a conical antirotating HAAKE twin-screw extruder (30 mm average screw diameter, 400 mm screw length, and screw speed of 150 rpm) operating at 220°C. The melt temperature increased to 230°C due to energy dissipation during extrusion.

Subsequent injection molding of round plates (80 mm diameter, 4 mm thick) was conducted with an ARBURG 221E/221P 175-35 E injection-molding machine. During injection molding, the barrel, die, and mold temperatures were maintained at 260°C, 280°C, and 70°C, respectively.

Characterization of Fracture Mechanics

The resistance to unstable crack initiation under dynamic loading conditions was evaluated with an instrumented Charpy impact tester with a maximum capacity of 4 J.[9,10] Single-edge notched-bend (SENB) specimens (width: W = 10 mm; thickness: B = 4 mm) were prepared from injection-molded plates, with the long beam dimension parallel to the injection flow direction. After cutting a sharp, 2-mm deep notch, these specimens were tested at room temperature with a pendulum hammer speed, v_H, of 1 m/s and a span, s, of 40 mm.

The toughness behavior was characterized with parameters of elastic–plastic fracture mechanics (EPFM). These parameters are independent of the specimen geometry, if minimum specimen geometry limits are utilized.[11–14] This enabled a conservative assessment of the toughness behavior. For specimens with different initial notch lengths, a, loaded under identical conditions, the J integral[15] was used to describe the difference of the potential energy resulting from differences in notch surfaces.[9,10] Several calculations were conducted using this energy-related interpretation of the J integral.[16–18] J-integral values describing the resistance to unstable crack initiation can be calculated using eq. (1):

$$J_{Id} = \frac{\eta_{el} A_{el}}{B(W-a)} + \frac{\eta_{pl} A_{pl}}{B(W-a)} \frac{W-(a+a_{BS})}{W-a} \quad (1)$$

where A_{el} and A_{pl} are elastic and plastic deformation energy, respectively; η_{el}, and η_{pl} are the elastic and plastic calibration function, respectively; and a_{BS} is stable crack growth. The experimental basis for this procedure involved measurements of force (F) versus deflection (f).[10]

The critical crack tip opening displacement (CTOD), δ_{Idk}, was used to quantify deformations near the notch:[19,20]

$$\delta_{Idk} = \frac{1}{n}(W-a)\frac{4f_k}{s} \quad (2)$$

where f_k is the notch component of the maximum deflection and n the rotational factor (n = 4, if crack propagation has become unstable).[10]

TEM and SEM Analyses

The morphology of the injection-molded blends was investigated by TEM. Ultrathin sections of about 60 nm thickness were stained with OsO_4 to make the polybutadiene phase visible. In addition one blend with a PB content of 10% wt was stained with RuO_4 to enhance the contrast between PPO and SAN. TEM measurements were performed on a Philips EM 400 instrument, using an accelerating voltage of 100 kV.

To determine correlations between morphology and toughness, a crack surface analysis was performed with optical and scanning electron microscopy. In order to facilitate viewing of three-dimensional deformation structures in SEM (Jeol JSM-6300), the fracture surfaces from the three-point bending specimens were mounted on 45°-sloped specimen targets.

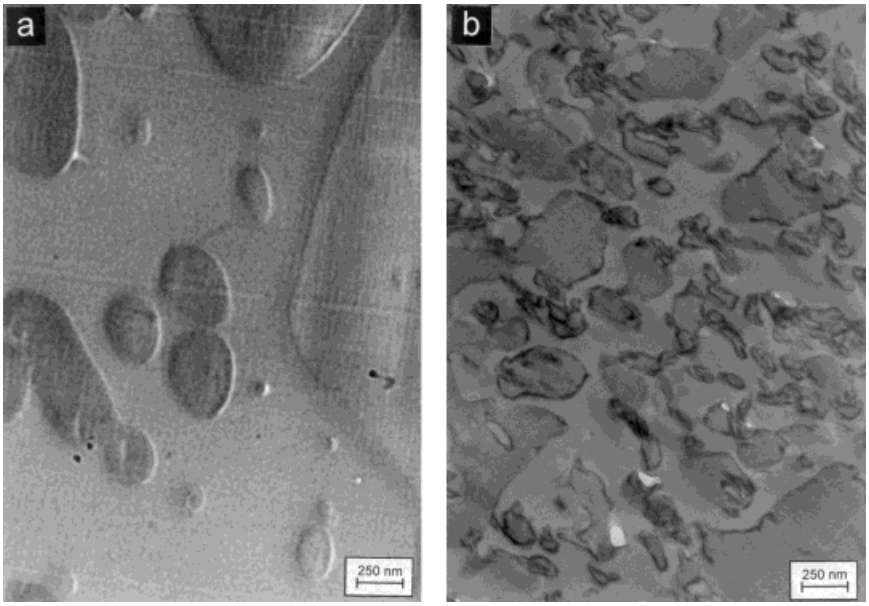

Figure 2 TEM micrographs of (a) PPO(+ HIPS)/SAN [light gray areas are SAN matrix; darker gray areas are PPO (+ HIPS) particles]; and (b) PPO (+ HIPS)/SAN/SBM (10 wt % rubber) [dark areas close to the particles are rubber phase].

RESULTS AND DISCUSSION

Morphology

As a consequence of the incompatibility and the high viscosity difference between PPO and SAN, dispersed PPO phases in the SAN matrix were expected. Due to the reduction of the interfacial tension in the compatibilized blend, the shapes of the PPO phases can deviate away from spheres, so that the minimum phase dimension should be smaller. Although the pure PPO–HIPS–SAN exhibited the expected morphology [Fig. 2(a)], some interesting morphological features were detected in the compatibilized blend [Fig. 2(b)].

With the qualification that shear orientation of PPO and SAN chains can be ignored, the morphology formed during extrusion process comes rather close to equilibrium. Because of the partial miscibility of PPO and PMMA as well as that of SAN and PS, SBM chains are orientated perpendicular relative to the PPO–SAN interface (the possibility of mixed phases formation depending on block lengths of polystyrene and poly(methyl methacrylate) blocks is demonstrated on example of poly(styrene methyl methacrylate) block copolymers (SM) by Auschra et al.[3]). As a consequence of the orientation of SBM chains polybutadiene has been able to reach the PPO–SAN interface only in the form of domains. These domains assume nearly spherical shape in order to minimize the interfacial area. Therefore, after the extrusion process, a distinct raspberry morphology with spherical PB phases at the interface was detected.

During injection molding, the morphology changed. The PPO–SAN interface was no longer regularly covered with polybutadiene spheres. Indeed, the interface contained no copolymer in many locations. The PPO phases had apparently grown and coalesced. The shape of the PB phases was no longer predominantly spherical.

High shear forces acting during injection molding have a great influence on the morphological development. Furthermore, there is a limited time period to drive the system to a new equilibrium. This leads to the formation of a nonequilibrium morphology corresponding to a "macrophase" separation of polybutadiene discussed in this article. Another possible reason for this morphology may be the crosslinking reactions of the polybutadiene that led to immobility of the triblock copolymers, which would thereby have inhibited the development of the thermodynamically most favored chain alignment at the interface.

Further addition of compatibilizer could result in the embedding of PPO particles by rubber, leading to the formation of classical core–shell structures. In addition, SBM micelles could be formed (a detailed discussion of SM–micelle formation in PPO is given by Auschra et al.[2] for

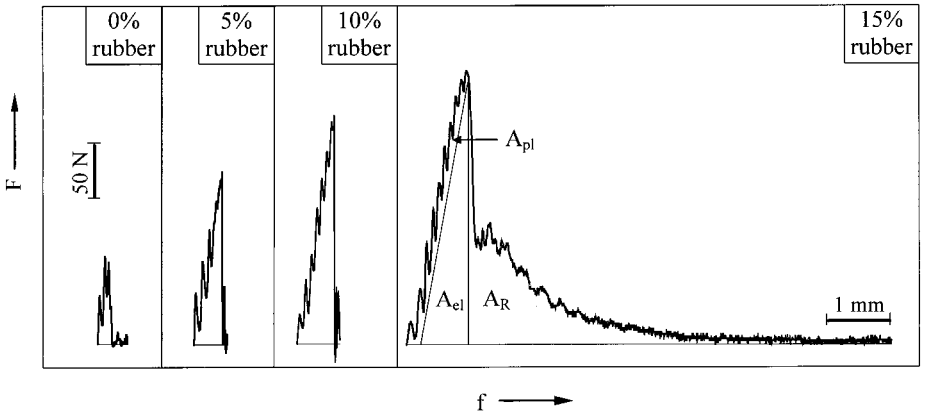

Figure 3 Force (F)-deflection (f) diagrams for PPO–SAN blends compatibilized with SBM with various rubber contents. A_{el} = elastic part of deformation energy; A_{pl} = plastic part of deformation energy; A_R = crack propagation energy.

PPO–SAN blends compatibilized with SM). Both the cases are, however, undesirable because these are neither economical nor do they improve the mechanical properties (see below). Which process is dominant—core–shell particles or micelle formation—cannot be clarified based on the present investigations.

More detailed discussions on the thermodynamics and microstructure of the blends can be found in the second part of this study.

Macroscopic Deformation and Fracture Behavior Under Impact-Loading Conditions

The measured *F-f* diagrams are plotted in Figure 3 for PPO–SAN blends with SBM as the coupling agent. These diagrams were the essential experimental basis for determining the toughness behavior. These results enable a first estimation of toughness level and fracture behavior. However, the determination of force-deflection behavior is exclusively qualitative since the behavior is geometry dependent. With increasing rubber content in the blends, both the maximum force, F_{max}, and deflection, f_{max}, increased in the same manner. Linear–elastic behavior with predominantly unstable crack propagation associated with a rapid change of the force was observed for blends containing up to 10% wt rubber (Fig. 3). Elastic–plastic behavior and a significant crack propagation energy, A_R, (A_R = 120 mJ) was observed for the blend with the highest rubber content; that is, for this specimen, a stable crack growth mechanism was dominant.

Corresponding blends modified with SBSB exhibited exclusively linear–elastic behavior. A very small crack propagation energy (A_R = 5 mJ) was measured only for the PPO–SAN + SBSB blend with 15% wt rubber.

In general, the shape of the force deflection diagrams cannot be quantitatively correlated with the extension of crack surface areas because of the strong geometry dependence of these areas. This geometry dependence is caused by a change of the working stress field. For example, the amount of stable crack propagation, detectable as the so-called stable crack growth, a_{BS}, after break of specimens, is the highest for plane stress.

However, the material behavior can be interpreted by analyzing respective crack surface phenomena. Figures 4(a)–(c) gives an overview of SEM micrographs of crack surfaces of PPO–SAN + SBM [Fig. 4(b)], PPO–SAN + SBSB both with 15% wt rubber [Fig. 4(c)], and the pure blend [Fig. 4(a)]. For the second type of specimen, a large stable crack growth (i.e., a stable crack surface with a high degree of plastic deformation and void formation corresponding to macroscopic stress whitening) was observed. In contrast, the planar and nearly undeformed fracture surface of PPO–SAN could be related to a brittle impact behavior. The largest plastic deformation, indicated by shear flow zones separated by shear lips, was found for the PPO–SAN + SBM specimens. SEM micrographs of microscopic details near the notch are presented in Fig. 4(d)–(f). For the unmodified blend, the dispersed PPO phase was exclusively deformed under loading as a consequence of large interparticle distances and the absence of adhesion between PPO and SAN [Fig. 4(d)]. Smoothly detached interfaces indicate that the extremely irregular PPO particles were only mechanically interlocked with the matrix.

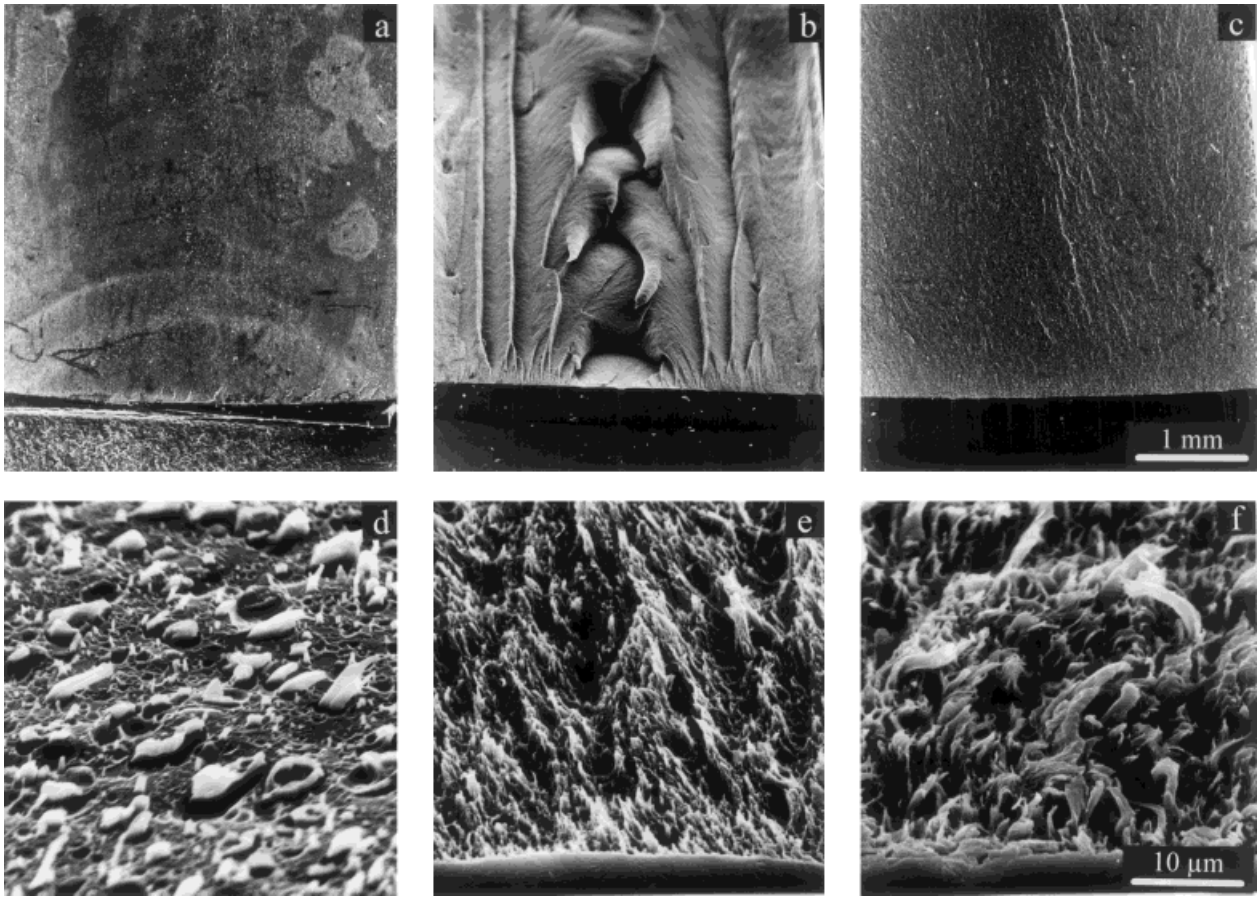

Figure 4 SEM micrographs of the macroscopic fracture surface (a–c) and corresponding details close to the initial notch (d–f) for PPO–SAN (a and d), PPO–SAN + SBM with 15% rubber (b and e) and PPO–SAN + SBSB with 15% rubber (c and f).

In contrast to the relatively weakly deformed SAN matrix, highly stretched PPO fibrils were observed for PPO–SAN + SBSB specimens [Fig. 4(f)]. For the PPO–SAN + SBM specimens, on the other hand, fibrillated, highly deformed material (both particles and matrix) was detected [Fig. 4(e)].

With the exception of pure PPO–SAN, stable crack growth (i.e., as a part of crack surface directly behind the notch) was observed for all blends (Fig. 5). As a consequence of an increase in the total deformation energy ($A_{el} + A_{pl}$), the values of a_{BS} for the blends increased with increasing rubber content. For the SBM-compatibilized blend with 15% wt rubber, a small unstable fracture area was found to have separated two different areas of stable crack propagation. This unstable fracture area was characterized by typical structures of high-speed crack propagation (e.g., arrest lines). The area close to the notch exhibited the common stable crack growth and could be related to the force deflection diagram for forces smaller than F_{max}. The length of damage area (a_{DL}) reflects the plastic zone separated during the fracture process. In principal, a_{DL} exhibited the same rubber content dependence as the a_{BS} values (Fig. 5).

For the blends with 15% wt rubber, different parametric trends representative of toughness behavior could be derived from the *F-f* diagrams (i.e., their shape and the amount of crack propagation energy) and the stable crack growth. This required the use of fracture mechanics parameters to quantify energy dissipation and deformation capacity. The rubber content dependence of the *J*-integral and CTOD values (shown in Fig. 6) for PPO–SAN + SBSB blends were different from that for PPO–SAN + SBM. The toughness of blends with the modifier SBSB reached their maximum value early in the deformation process, while blends with SBM still have a huge toughness potential. On the one hand, this can be illustrated in the light of highly sloped toughness versus rubber content curves plotted on the left side in Figure 6, from which can be assumed a contin-

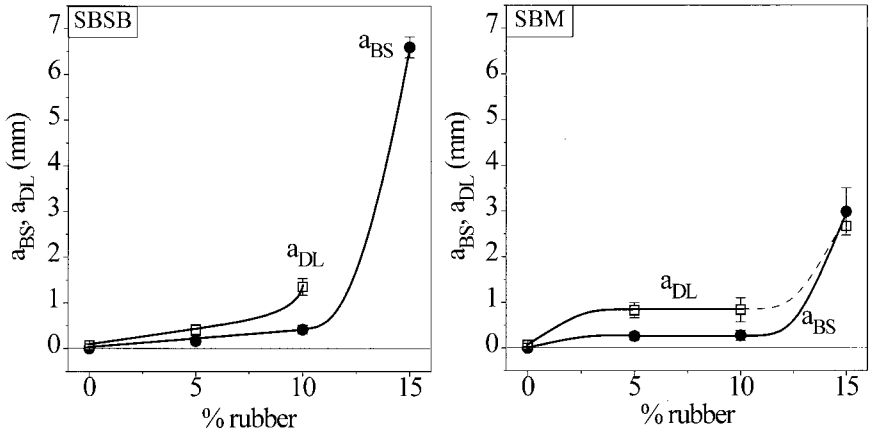

Figure 5 Stable crack growth and length of damage area, a_{BS} (●) and a_{DL} (□), respectively, as a function of rubber content for PPO–SAN blends compatibilized with SBSB and SBM (for PPO–SAN + SBM with 15% rubber, the damage area could be observed for only one specimen).

ual increasing of toughness values for rubber content higher than 15%. On the other hand, the formation of high crack propagation energy for PPO–SAN + SBM with 15% rubber, which can be seen in Figure 3, means the fracture process is more stable than for PPO–SAN + SBSB.

As mentioned earlier, the relation between stiffness and toughness is of critical importance for the application of polymeric materials. The dynamic Young's modulus, E_d (an indicator of stiffness; also plotted in Fig. 6) can be calculated using eq. (3):

$$E_d = \frac{F_{GY} s^3}{4 f_{GY} B W^3} \tag{3}$$

F_{GY} and f_{GY} represent the force and corresponding deflection at the transition point from elastic to elastic–plastic behavior, respectively. For materials exhibiting only elastic behavior, F_{max} and f_{max} should be replaced by F_{GY} and f_{GY}, respectively. It is very interesting that the incorporation of a high amount of rubber (up to 15% wt) into the PPO–SAN blends modified with SBM

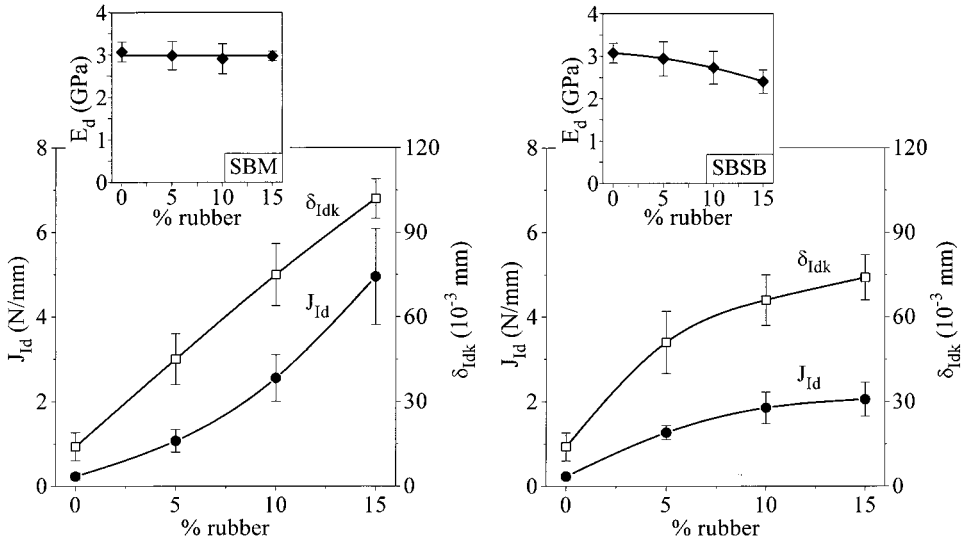

Figure 6 Fracture mechanics parameters, J_{Id} (●) and δ_{dk} (□), and dynamic Youngs's moduli, E_d (♦), (small figures) plotted against the rubber content for PPO–SAN blends compatibilized with SBSB and SBM.

resulted in a dramatic increase in toughness without a significant decrease in modulus.

The values of Young's modulus (E_d = 3 GPa) remained at the same high level as for the nonmodified material. This behavior, which contrasts with conventional toughened materials like ABS, is caused by the special microstructure of these blends. For the case of a stiff polymeric matrix containing stiff particles enclosed into a rubber shell (core–shell particles), the external load is easily transferred only into the shell but not into the particle core. A low stiffness can be expected for such a material.

In contrast, a relatively high energy dissipation is observed in SBM-modified PPO–SAN blends. This is caused by cavitation near the PPO–SAN interface, which is associated with the shear deformation of the SAN matrix resulting from a high stretching of the microphase-separated rubber. Direct contact between PPO and SAN, on the other hand, also contributes to the high stiffness.

In contrast to the SBM-modified blends, the E_d values for the SBSB-modified blends decreased slightly with increasing rubber content. Figure 7(a,b) demonstrates the relationship between relative stiffness and toughness behavior of various materials. In this figure, Young's modulus (in units of the stiffness parameter, E_{d0}, of the "matrix" materials) is plotted against the toughness parameter (in units of the "matrix" material parameters, J_{Id}/J_{Id0} and $\delta_{Idk}/\delta_{Idk0}$). The behavior of toughened PPO–SAN blends was compared with that of various ABS materials (rubber content: 0–36%).[21,22] The obtained values for these conventional rubber-modified materials (especially for ABS with a particle diameter of about 110 nm) were located at the upper limit of the relationship between stiffness and toughness. This latter limit could be approximated by $E_d/E_{d0} = J_{Id0}/J_{Id}$ [Fig. 7(a)] and $E_d/E_{d0} = \delta_{Idk0}/\delta_{Idk}$ [Fig. 7(b)]. Because PPO–SAN + SBM blends behave in an opposite manner, a rare combination of stiffness and toughness was observed. The energy dissipation up to the maximum force and the deformation capacity of a pure PPO–SAN blend could be increased by a factor of 20 and 7, respectively, by using SBM as a compatibilizer.

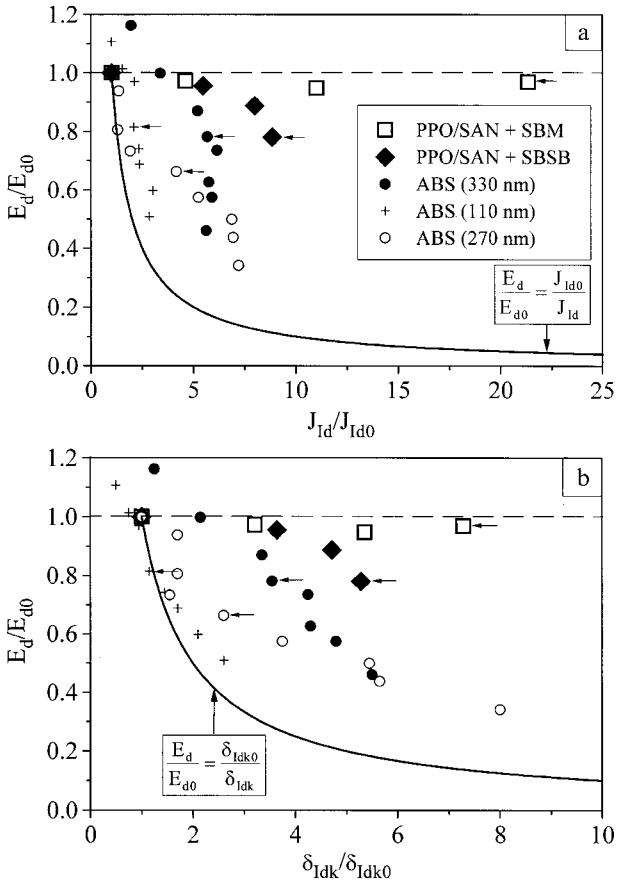

Figure 7 Relationship between relative stiffness, E_d/E_{d0}, and relative toughness parameters (a) J_{Id}/J_{Id0} and (b)$\delta_{Idk}/\delta_{Idk0}$ for various toughened materials (PPO–SAN blends compatibilized with SBM (□) and SBSB (♦); ABS materials with an average particle diameter of 330 nm (●), 110 nm (+) and 270 nm (○).[21,22] Full line represents limiting curves of toughness modification; broken line represents ideal curve of toughened plastics. E_{d0}, J_{Id0}, and δ_{Idk0} are the corresponding values of the "matrix" materials. Arrows indicate the comparison of the stiffness–toughness behavior of ABS materials with 16% rubber and PPO–SAN blends with 15% rubber.

CONCLUSIONS

A relatively low stiffness for materials with conventional core–shell particles (stiff polymeric matrix containing stiff particles fully enclosed into a rubber shell) can be expected. This behavior corresponds with fracture behavior that was not strongly dependent on the rubber content.

In contrast to this, it has been shown in this study with an example of PPO–SAN blends with the modifier SBM that both direct contact between particles (PPO) and matrix (SAN) and a particle-matrix interface in which rubber phase is discontinuously accumulated are necessary to get a highly stiffness-leveled material where Young's modulus is nearly independent of rubber content. We also found that relatively high energy dissipation up to maximum force (up to about 20 times higher energy compared to pure PPO–SAN blends) caused by cav-

itation near the PPO–SAN interface is associated with the shear deformation of the SAN matrix resulting from a high stretching rubber phase.

Thus, a way can be demonstrated to develop new polymeric materials that combine high modulus with high toughness.

The authors wish to thank Professor Michler for making possible SEM investigations.

REFERENCES

1. Bucknall, C. B. Toughened Plastics; Applied Science: London, 1977.
2. Auschra, C.; Stadler, R.; Voigt-Martin, I. G. Polymer 1993, 34, 2081.
3. Auschra, C.; Stadler, R.; Voigt-Martin, I. G. Polymer 1993, 34, 2094.
4. Beckmann, J.; Auschra, C.; Stadler, R. Macromol Rapid Commun 1994, 15, 67.
5. Stadler, R.; Krappe, U.; Breiner, U. Polymer Preprints 1996, 37, 434.
6. Auschra, C.; Stadler, R. Macromolecules 1993, 26, 6364.
7. Green, F. P.; Russel, T. P.; Jerome, R.; Granville, M. Macromolecules 1988, 21, 3266.
8. Auschra, C.; Stadler, R. Polymer Bulletin 1993, 30, 257.
9. Grellmann, W.; Sommer, J.-P.; Hoffmann, H.; Michel, B. 1st Conference on Mechanics, Proc 1987, 5, 129.
10. Grellmann, W.; Seidler, S. J Polymer Eng 1992, 11, 71.
11. Grellmann, W.; Seidler, S. Intern J Fract 1994, 68, R19.
12. Grellmann, W.; Seidler, S.; Lauke, B. Polymer Compos 1991, 12, 320.
13. Grellmann, W.; Che, M. J Appl Polymer Sci 1997, 66, 1237.
14. Lach, R. Korrelationen zwischen bruchmechanischen Werkstoffkenngrössen und molekularen Relaxationsprozessen polymerer Werkstoffe; VDI-Verlag; Düsseldorf, 1998.
15. Rice, J. R. Trans, J Appl Mech 1968, 35, 379; Rice, J. R. In Fracture; Academic Press: New York, 1968; Vol. II.
16. Begley J. A.; Landes, J. D. ASTM STP 1973, 536, 246.
17. Merkle, H. C.; Corten, H. T. J Pressure Vessel Technol 1974, 96, 286.
18. Sumpter, J. D. G.; Turner, C. E. ASTM STP 1976, 3, 601.
19. Grellmann, W.; Jungbluth, M. Fracture Mechanics, Micromechanics and Coupled Fields (FMC-Series) 1987, 37, 186.
20. Grellmann, W.; Lach, R. Appl Macromol Chem Phys 1996, 237, 191.
21. Lach, R.; Han, Y.; Grellmann, W.; Krüger, P. In Deformation and Fracture Behaviour of Plastics; Grellmann, W., Seidler, S. Eds.; Springer: Berlin, Heidelberg, 2000.
22. Han, Y.; Lach, R.; Grellmann, W. Appl Macromol Chem Phys 1999, 270, 13.